High-spin states in ^{127}Ce and ^{129}Ce: Further evidence for triaxial nuclear shapes

E. S. Paul,[1] J. P. Revill,[1] M. Mustafa,[1] S. V. Rigby,[1] A. J. Boston,[1] C. Foin,[2] J. Genevey,[2] A. Gizon,[2] J. Gizon,[2] I. M. Hibbert,[3] D. T. Joss,[1] P. J. Nolan,[1] B. M. Nyakó,[4] N. J. O'Brien,[3] C. M. Parry,[3] A. T. Semple,[1] S. L. Shepherd,[1] J. Timár,[4] R. Wadsworth,[3] and L. Zolnai[4]

[1]*Oliver Lodge Laboratory, University of Liverpool, Liverpool L69 7ZE, United Kingdom*
[2]*Institut des Sciences Nucléaires, IN2P3-CNRS/Université Joseph Fourier, Grenoble, France*
[3]*Department of Physics, University of York, Heslington, York YO10 5DD, United Kingdom*
[4]*Institute of Nuclear Research, H-4001 Debrecen, Hungary*

(Received 21 August 2009; published 19 November 2009)

High-spin states have been studied in the neutron-deficient odd-N ^{127}Ce and ^{129}Ce isotopes, produced in ^{100}Mo(^{32}S,5$n\gamma$) and ^{100}Mo(^{34}S,5$n\gamma$) reactions, using the Euroball and Eurogam γ-ray spectrometers, respectively. A quadruples analysis (γ^4) of the coincident γ-ray data has established new band structures in ^{127,129}Ce and extended the known bands to higher spin. In addition, links have been established between two positive-parity bands in ^{127}Ce allowing a reassignment of $I^\pi = 1/2^+$ to the ground state of this nucleus. Configuration assignments are made by comparison of band properties with cranked Woods-Saxon calculations and systematics of other light odd-N cerium isotopes. Unusually large signature splitting in the negative-parity bands is discussed in terms of nonaxial nuclear shapes induced by the core-polarization effects of $h_{11/2}$ neutrons.

DOI: 10.1103/PhysRevC.80.054312 PACS number(s): 21.10.Re, 27.60.+j, 23.20.Lv

I. INTRODUCTION

An ongoing quest in nuclear-structure physics is to experimentally establish static triaxial shapes, i.e., nuclei with distinct "short," "intermediate," and "long" principal axes. The rotation of such asymmetric bodies can exhibit a "wobbling" motion, similar to the precession of the Earth. Indeed, such wobbling motion has long been predicted to occur in nuclei at high spin [1,2] and evidence for such behavior has been presented for Lu nuclei [3,4]. At low spin, the energy differences between the two signature components of rotational bands built on high-j, high-Ω orbitals in odd-A nuclei, i.e., the "signature splitting," is highly sensitive to the degree of triaxiality. Such nuclei with the requisite properties generally lie just below major shell closures; prime examples include mass 130 nuclei with $N \sim 75$ (below $N = 82$) and mass 160 nuclei with $Z \sim 75$ (below $Z = 82$).

The ground states of the lightest neutron-deficient cerium ($Z = 58$) isotopes with $A < 128$ are predicted to possess well-deformed *axially symmetric* prolate shapes with $\beta_2 =$ 0.25–0.30 [5]. However, *nonaxial* shapes, described by the triaxiality parameter γ in the polar representation of rotating quadrupole shapes [2], are thought to become important for the heavier cerium isotopes beyond $A = 130$ and approaching the $N = 82$ shell closure [6–8]. Such nonaxial nuclear deformation is induced through "core polarization" by valence particles in anisotropic orbitals [9,10]. For instance, high-j particles from the bottom of a subshell prefer prolate nuclear shapes, while particles from the top of a subshell prefer an oblate shape [11]. The delicate interplay of such valence particles can therefore influence the overall shape of the nucleus, inducing triaxiality. Such is the case for the neutron-deficient cerium isotopes where valence protons occupy low-Ω orbitals from the bottom of the $\pi h_{11/2}$ subshell, while valence neutrons occupy high-Ω orbitals from the top of the $\nu h_{11/2}$ subshell. Hence these nuclei provide an ideal environment for studying the shape-driving effects of specific valence particles.

In the light odd-N cerium isotopes around mass 130, the yrast bands at low spin correspond to negative-parity high-j $h_{11/2}$ orbitals with high-Ω values of $7/2$ or $9/2$. Such orbitals are expected to show vanishingly small signature splitting, for prolate shapes, as seen for positive-parity bands in these nuclei at low spin. However, bands based on these high-Ω $h_{11/2}$ orbitals exhibit unusually large values of signature splitting at low spin, which decrease as low-Ω $h_{11/2}$ protons align at higher spin. The opposite core polarizations induced by the $h_{11/2}$ neutrons and protons may be responsible for such behavior.

This article presents new results for the odd-N ^{127}Ce and ^{129}Ce isotopes obtained using the Euroball and Eurogam multidetector γ-ray spectrometers, respectively. Woods-Saxon cranking calculations are used to interpret the band structures in these nuclei and the results are also compared to neighboring odd-N cerium isotopes. Measured $B(M1)/B(E2)$ ratios of reduced transition probabilities are also compared to theory to strengthen the configuration assignments.

II. EXPERIMENTAL DETAILS AND RESULTS

A. The Euroball experiment for ^{127}Ce

High-spin states in $^{127}_{58}$Ce$_{69}$ were populated using the ^{32}S + ^{100}Mo fusion-evaporation reaction, carried out at the Legnaro National Laboratories, Italy. The XTU tandem accelerator provided a 155-MeV ^{32}S beam to bombard two stacked self-supporting foils of ^{100}Mo (>97% enriched), each of nominal thickness 600 μg/cm^2; ^{127}Ce was populated via the ^{100}Mo(^{32}S,5$n\gamma$) channel. Coincident escape-suppressed, high-fold γ-ray events, within a prompt time window of 50 ns, were collected using the Euroball spectrometer [12]. The present experiment was one of the first with this spectrometer, which contained 27 coaxial [13], 25 four-element clover [14], and 13 seven-element cluster [15] HPGe detectors.

A total of 1.3×10^9 events (γ^n, $n \geqslant 5$) were recorded to tape in 32 h for subsequent off-line analysis. Given the neutron-deficient nature of the compound nucleus (^{132}Ce*), significant charged-particle evaporation competed with pure neutron evaporation and many nuclei were populated with $Z = 54$–58. The strongest channel observed was the $p4n$ channel into ^{127}La; the $5n$ channel (^{127}Ce) was measured as 20% of the ^{127}La strength, while the $4n$ channel (^{128}Ce) was measured as 60%. Results for both ^{127}La [16] and ^{128}Ce [17] have previously been published from this work.

To investigate the high-spin level schemes of nuclei populated in this experiment, the high-fold data were unfolded off-line into constituent quadruple (γ^4) coincidence events, software gain matched, and replayed into a RADWARE 4-D hypercube with a nonlinear gain [18] of 3.3 channels/full width at half maxiumum. γ rays with energies from 0.1 MeV up to 2.5 MeV were stored in the hypercube, which had 1375 channels per dimension. Approximately five quadruples per event were found, leading to a total of 7×10^9 events incremented into the hypercube. Analysis was conducted using 4dg8r part of the RADWARE graphical analysis package [19]. Three simultaneous gates, or indeed lists of gates, can be placed on the x, y, and z axes of the hypercube and the w axis projected into a one-dimensional spectrum.

The level scheme deduced for ^{127}Ce from the present work is shown in Fig. 1, where the transitions have been arranged into three band structures, labeled 1–3. A suffix "a" is added to the labels for the bands above the first backbend. The ordering of transitions in the decay scheme is based on relative γ-ray intensities and quadruple (γ^4) coincidence relationships. Examples of triple-gated coincidence spectra are presented in Fig. 2 for the bands shown in Fig. 1. γ-ray energies, relative intensities, and assumed spin/parity assignments are listed in Table I, Table II, and Table III, respectively, for the transitions in the three band structures. The spin and parity of the lower levels are taken from previous work [20] and the in-band transitions are assumed to be of stretched $E2$ character.

Previously, three transitions at the bottom of Band 1 were assigned to ^{127}Ce following work with the Daresbury recoil separator [21]. Subsequent work extended this band and identified transitions in Band 2 [22]. The assignment of these two bands to ^{127}Ce was confirmed through decay studies of ^{127}Pr using β-gated and x-ray-gated γ-ray spectra [23]. A transition of energy 29.6 keV, observed in another β-decay study of ^{127}Pr [24], has been placed linking the bandheads of Bands 1 and 2 [20]. In addition, these β-decay studies identified the lowest transitions of Band 3 [23,24], although this structure was not linked to the other two bands. It was assumed that the band-head of Band 2 represented the ground-state of ^{127}Ce with spin-parity $I^\pi = 5/2^+$ [20]. Moreover, β-decay studies of ^{127}Ce itself identified two activities of 29 ± 2 s and 34 ± 2 s, which were attributed to closely lying $I^\pi = 5/2^+$ and $1/2^+$ states, respectively [25].

The present work has extended all three band structures to higher spin, particularly Bands 2 and 3. Band 1, previously observed up to $51/2^-$, has been extended to $57/2^-$. Band 2, previously observed up to $25/2^+$, has been significantly extended (Band 2a) up to $53/2^-$. The lower members of Band 3 up to $7/2^+$ were previously identified in β-decay studies of ^{127}Pr [23]. This band has now been extended to

TABLE I. Energies, intensities, and proposed spin-parity assignments for the transitions assigned to Bands 1 and 1a in ^{127}Ce.

E_γ (keV)[a]	I_γ	Assignment
	Bands 1, 1a dipoles	
125.5	55(5)	$9/2^- \to 7/2^-$
162.3	152(5)	$11/2^- \to 9/2^-$
220.8	77(3)	$15/2^- \to 13/2^-$
227.7	84(3)	$13/2^- \to 11/2^-$
254.9	67.8(22)	$27/2^- \to 25/2^-$
255.9	13.7(16)	$31/2^- \to 29/2^-$
257.0	35.0(16)	$19/2^- \to 17/2^-$
275.3	24.8(10)	$23/2^- \to 21/2^-$
320.2	36.1(22)	$17/2^- \to 15/2^-$
321.0	32.2(16)	$35/2^- \to 33/2^-$
330.1	51.4(22)	$29/2^- \to 27/2^-$
332.0	41.0(22)	$33/2^- \to 31/2^-$
386.6	29.8(11)	$37/2^- \to 35/2^-$
392.8	14.1(12)	$39/2^- \to 37/2^-$
400.9	33.3(22)	$21/2^- \to 19/2^-$
430.9	30.1(16)	$25/2^- \to 23/2^-$
451.0	24.6(22)	$41/2^- \to 39/2^-$
458.3	16(3)	$43/2^- \to 41/2^-$
516.5	8.2(16)	$45/2^- \to 43/2^-$
512.4	10.9(16)	$47/2^- \to 45/2^-$
	Bands 1, 1a quadrupoles	
288.3	46.4(22)	$11/2^- \to 7/2^-$
390.1	45.4(16)	$13/2^- \to 9/2^-$
448.8	≡100	$15/2^- \to 11/2^-$
541.7	74(3)	$17/2^- \to 13/2^-$
577.3	181(7)	$19/2^- \to 15/2^-$
585.3	56(3)	$29/2^- \to 25/2^-$
585.9	135(8)	$31/2^- \to 27/2^-$
589.3	42.1(22)	$33/2^- \to 29/2^-$
652.4	67(4)	$35/2^- \to 31/2^-$
658.1	72(4)	$21/2^- \to 17/2^-$
676.7	191(7)	$23/2^- \to 19/2^-$
686.7	140(6)	$27/2^- \to 23/2^-$
706.9	71(6)	$25/2^- \to 21/2^-$
708.0	53(5)	$37/2^- \to 33/2^-$
779.8	78(7)	$39/2^- \to 35/2^-$
842.0	56(4)	$41/2^- \to 37/2^-$
908.0	74(8)	$43/2^- \to 39/2^-$
973.5	60(8)	$45/2^- \to 41/2^-$
1030.2	82(9)	$47/2^- \to 43/2^-$
1101.6	63(10)	$49/2^- \to 45/2^-$
1139.9	41(11)	$51/2^- \to 47/2^-$
1222.7	60(11)	$53/2^- \to 49/2^-$
1242.4	39(11)	$55/2^- \to 51/2^-$
1337.0	11(10)	$57/2^- \to 53/2^-$
1337.0		$59/2^- \to 55/2^-$

[a]The γ-ray energies are estimated to be accurate to ±0.3 keV for the strong transitions ($I_\gamma > 10$), rising to ±0.6 keV for the weaker transitions.

TABLE II. Energies, intensities, and proposed spin-parity assignments for the transitions assigned to Bands 2 and 2a in ^{127}Ce.

E_γ (keV)[a]	I_γ[b]	Assignment
	Bands 2, 2a dipoles	
159.5	55(5)	$7/2^+ \to 5/2^+$
198.5	39.3(16)	$9/2^+ \to 7/2^+$
234.8	25.1(16)	$11/2^+ \to 9/2^+$
265.4	22.3(10)	$13/2^+ \to 11/2^+$
274.3	6.7(5)	$27/2^+ \to 25/2^+$
294.5	9.6(9)	$15/2^+ \to 13/2^+$
300.2	13.3(8)	$29/2^+ \to 27/2^+$
311.6	22.8(13)	$31/2^+ \to 29/2^+$
316.6	13.9(10)	$17/2^+ \to 15/2^+$
328.4	11.7(12)	$19/2^+ \to 17/2^+$
333.9	15(3)	$25/2^+ \to 23/2^+$
334.9	15(3)	$21/2^+ \to 19/2^+$
336.6	8.6(13)	$33/2^+ \to 31/2^+$
345.8	9.9(10)	$23/2^+ \to 21/2^+$
	Bands 2, 2a quadrupoles	
359.2	30.1(22)	$9/2^+ \to 5/2^+$
433.5	13.6(10)	$11/2^+ \to 7/2^+$
500.7	35.5(22)	$13/2^+ \to 9/2^+$
559.8	47(3)	$15/2^+ \to 11/2^+$
575.5	25(3)	$29/2^+ \to 25/2^+$
609.9	46(4)	$27/2^+ \to 23/2^+$
611.6	16(3)	$17/2^+ \to 13/2^+$
611.7	50(4)	$31/2^+ \to 27/2^+$
647.3	26(4)	$33/2^+ \to 29/2^+$
650.5	55(5)	$19/2^+ \to 15/2^+$
667.4	21(3)	$21/2^+ \to 17/2^+$
680.2	33(7)	$25/2^+ \to 21/2^+$
682.1	43(7)	$23/2^+ \to 19/2^+$
716.9	27(4)	$35/2^+ \to 31/2^+$
783.6	26(4)	$37/2^+ \to 33/2^+$
820.7	22(5)	$39/2^+ \to 35/2^+$
868.6	25(7)	$41/2^+ \to 37/2^+$
896.7	19(7)	$43/2^+ \to 39/2^+$
923.0	34(7)	$45/2^+ \to 41/2^+$
951.2	14(7)	$47/2^+ \to 43/2^+$
997.8	24(8)	$49/2^+ \to 45/2^+$
1043.8	14(8)	$51/2^+ \to 47/2^+$
1089.9	10(5)	$53/2^+ \to 49/2^+$

[a]The γ-ray energies are estimated to be accurate to ± 0.3 keV for the strong transitions ($I_\gamma > 10$), rising to ± 0.6 keV for the weaker transitions.
[b]The intensities are given relative to the 448.8-keV $15/2^- \to 11/2^-$ transition of Band 1 ($\equiv$100).

TABLE III. Energies, intensities, and proposed spin-parity assignments for the transitions assigned to Bands 3 and 3a in ^{127}Ce.

E_γ (keV)[a]	I_γ[b]	Assignment
	Bands 3, 3a dipoles	
176.1	55(16)	$5/2^+ \to 3/2^+$
254.8[c]	4.2(4)	$\to 23/2^+$
298.5	4.5(12)	$9/2^+ \to 7/2^+$
311.6[c]	2.8(3)	$27/2^+ \to$
399.3	28(5)	$13/2^+ \to 11/2^+$
466.2	1.6(22)	$17/2^+ \to 15/2^+$
	Bands 3, 3a quadrupoles	
205.1	37(4)	$5/2^+ \to 1/2^+$
242.9	82(4)	$7/2^+ \to 3/2^+$
365.6	20.8(16)	$9/2^+ \to 5/2^+$
402.9	37(11)	$11/2^+ \to 7/2^+$
501.8	36(3)	$13/2^+ \to 9/2^+$
518.0	19.1(22)	$27/2^+ \to 23/2^+$
534.9	19.7(16)	$25/2^+ \to 21/2^+$
540.6	42(3)	$15/2^+ \to 11/2^+$
561.9	29(3)	$27/2^+ \to 23/2^+$
565.7[c]	21.3(16)	$27/2^+ \to 23/2^+$
572.6	38(4)	$31/2^+ \to 27/2^+$
609.8	35(5)	$17/2^+ \to 13/2^+$
646.9	27(5)	$21/2^+ \to 17/2^+$
649.9	44(6)	$19/2^+ \to 15/2^+$
675.0	24(5)	$23/2^+ \to 19/2^+$
682.6	27(4)	$33/2^+ \to 29/2^+$
700.9	29(7)	$35/2^+ \to 31/2^+$
814.2	27(5)	$37/2^+ \to 33/2^+$
835.3	27(6)	$39/2^+ \to 35/2^+$
958.2	23(10)	$41/2^+ \to 37/2^+$
964.1	26(13)	$43/2^+ \to 39/2^+$

[a]The γ-ray energies are estimated to be accurate to ± 0.3 keV for the strong transitions ($I_\gamma > 10$), rising to ± 0.6 keV for the weaker transitions.
[b]The intensities are given relative to the 448.8-keV $15/2^- \to 11/2^-$ transition of Band 1 ($\equiv$100).
[c]Transition linking Band 3 to Band 2.

$43/2^+$. In addition, linking transitions have been established between Bands 2 and 3; a 566-keV transition links the $27/2^+$ state of Band 3a to the $23/2^+$ state of Band 2. A parallel branch (255–311 keV) also links these states. With these links, the $I^\pi = 1/2^+$ bandhead of Band 3 lies 7 keV below the $I^\pi = 5/2^+$ band-head of Band 2, and hence the ground state of ^{127}Ce is now reassigned to have spin-parity $I^\pi = 1/2^+$. This assignment is, however, consistent with the ^{125}Ba isotone that also has a ground-state spin-parity $I^\pi = 1/2^+$ [26,27]. In addition, a low-lying $I^\pi = 1/2^+$ state, possibly the ground state, is also known in the ^{129}Nd isotone [28].

B. The Eurogam experiment for ^{129}Ce

High-spin states in $^{129}_{58}Ce_{71}$ were populated using the ^{34}S + ^{100}Mo fusion-evaporation reaction carried out at the Centre de Recherches Nucléaires, Strasbourg, France. The Vivitron electrostatic accelerator provided a 155-MeV ^{34}S beam to bombard two stacked self-supporting foils of ^{100}Mo (>97% enriched), each of nominal thickness 600 μg/cm^2; ^{129}Ce was populated via the ^{100}Mo(^{34}S,5$n\gamma$) channel. Coincident escape-suppressed, high-fold γ-ray events, within a prompt time window of 50 ns, were collected using the Eurogam 2 spectrometer equipped with 30 tapered coaxial, and 24 four-element clover, escape-suppressed HPGe detectors [29].

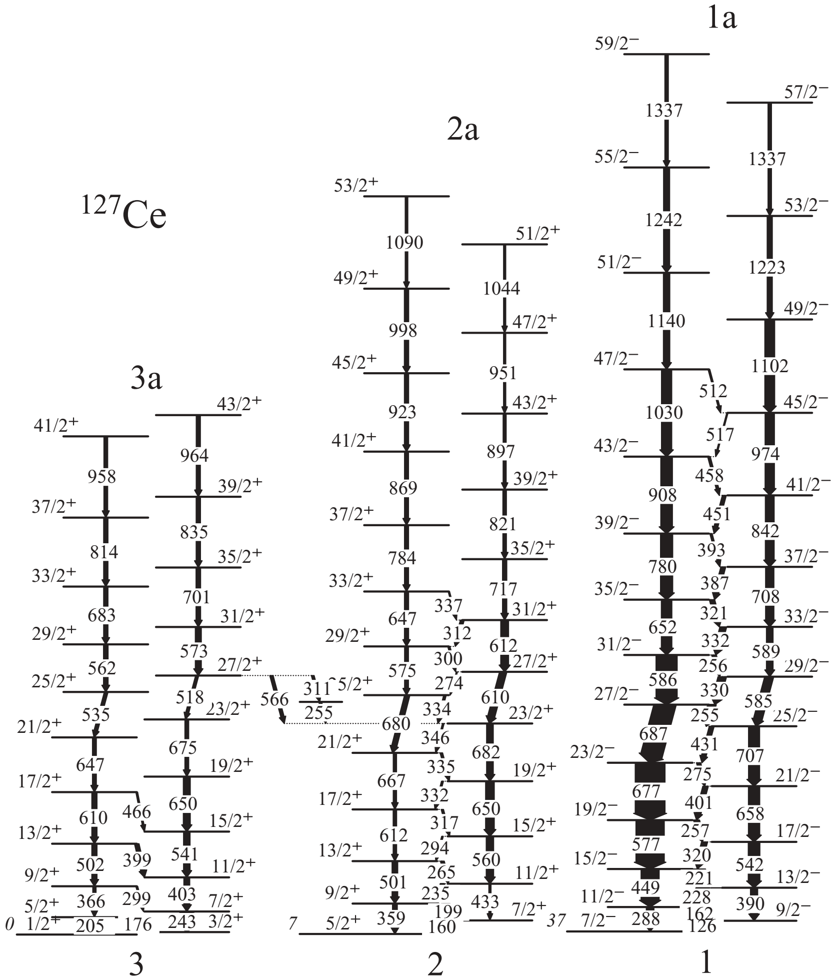

FIG. 1. Level scheme deduced for ^{127}Ce from the present work. Energies are labeled in keV and the widths of the arrows are proportional to the transition intensities. The energies of the lowest state in each band are also labeled, with the $I^{\pi} = 1/2^{+}$ state of Band 3 assigned as the ground state of this nucleus.

Approximately 8×10^{8} Compton-suppressed, high-fold γ-ray coincidences (γ^{n}, $n \geqslant 5$) were recorded to tape. The data were unpacked off-line into quadruple coincidences (γ^{4}) coincidence events, software gain matched, and replayed into a RADWARE 4-D hypercube. Analysis was again conducted using the 4dg8r program. The strongest channel observed was the $4n$ channel into ^{130}Ce; the $5n$ channel (^{129}Ce) was measured as 20% of the ^{130}Ce strength. Results for ^{130}Ce [30] have previously been published from this experiment.

The level scheme deduced for ^{129}Ce from the present work is shown in Fig. 3. Again, the ordering of transitions in the decay scheme is based on relative γ-ray intensities and quadruple (γ^{4}) coincidence relationships. Examples of triple-gated coincidence spectra are presented in Fig. 4 for the bands shown in Fig. 3. Gamma-ray energies, relative intensities, and assumed spin/parity assignments are listed in Table IV, Table V, and Table VI, respectively. The spin and parity of the lower levels of Bands 1–3 are taken from previous work [31] and the in-band transitions are assumed to be of stretched $E2$ character.

Previous work on ^{129}Ce established Bands 1 and 2 at low spin, together with a linking transition between them [32,33]. The bandhead of Band 1 was found to be isomeric with a half-life $T_{1/2} \approx 62$ ns [32]. Subsequently, these bands were extended (Bands 1a and 3) and decoupled Band 4 was identified [34]; an enhanced quadrupole deformation was deduced for this latter band from measured level lifetimes [34]. The present work has extended all these bands to higher spin and established a new structure, namely Band 2a in Fig. 3. Similar to previous work [34], Band 4 could not be definitely linked into the other band structures but clearly feeds only the lower members of Band 2, see Fig. 4(d). The present γ^{4} coincidence analysis has better defined the decay path of Band 4 into Band 2 with respect to Ref. [34]. For instance, the 547-keV transition at the bottom of Band 4 is in coincidence only with the two lowest dipole transitions of Band 2, with energies 145 and 204 keV. A weak transition of energy 420 keV is placed below the 547-keV transition [see Fig. 4(d)] and is assumed to be the continuation of the band to lower spin. The intensity of Band 4 peaks at the 601-keV transition (10%) and drops off for the lower-spin 547- and 420-keV transitions. A tentative bandhead spin and parity assignment of $I^{\pi} = (9/2^{-})$ is made to Band 4 based on theoretical expectations (see Sec. III A1).

β-decay studies of ^{129}Pr also established six members of a band built on an $I^{\pi} = 1/2^{+}$ state, which is almost degenerate with the $I^{\pi} = 5/2^{+}$ ground state of ^{129}Ce [35]. This structure,

TABLE IV. Energies, intensities, and proposed spin-parity assignments for the transitions assigned to Bands 1 and 1a in ^{129}Ce.

E_γ (keV)[a]	I_γ	Assignment
	Bands 1, 1a dipoles	
82.3	>110	$9/2^- \to 7/2^-$
107.8[b]	30(3)[c]	$7/2^+ \to 5/2^-$
145.7	89.0(28)	$11/2^- \to 9/2^-$
210.2	47.4(20)	$15/2^- \to 13/2^-$
224.3	17.2(11)	$27/2^- \to 25/2^-$
236.0	18.0(14)	$19/2^- \to 17/2^-$
241.4	10.8(12)	$23/2^- \to 21/2^-$
253.1	92.0(36)	$31/2^- \to 29/2^-$
260.7	73.8(32)	$13/2^- \to 11/2^-$
318.5	56.0(21)	$29/2^- \to 27/2^-$
327.1	48.6(20)	$33/2^- \to 31/2^-$
329.2	41.3(18)	$35/2^- \to 33/2^-$
381.2	21.3(17)	$17/2^- \to 15/2^-$
390.0	25.0(13)	$37/2^- \to 35/2^-$
403.4	21.4(14)	$39/2^- \to 37/2^-$
456.3	18.0(26)	$41/2^- \to 39/2^-$
469.9	16.2(14)	$43/2^- \to 41/2^-$
486.6	14.9(17)	$21/2^- \to 19/2^-$
515.2		16.9(18) $25/2^- \to 23/2^-$
524.5	7.2(12)	$45/2^- \to 43/2^-$
	Bands 1, 1a quadrupoles	
228.2	53.8(12)	$11/2^- \to 7/2^-$
405.8	19.1(12)	$13/2^- \to 9/2^-$
470.7	79.2(28)	$15/2^- \to 11/2^-$
542.7	26.3(16)	$29/2^- \to 25/2^-$
571.4	28.5(19)	$31/2^- \to 27/2^-$
579.9	19.2(16)	$33/2^- \to 29/2^-$
591.2	45.9(29)	$17/2^- \to 13/2^-$
616.5	≡100	$19/2^- \to 15/2^-$
656.3	25.4(17)	$35/2^- \to 31/2^-$
719.1	16.0(16)	$37/2^- \to 33/2^-$
722.3	31.3(21)	$21/2^- \to 17/2^-$
727.9	92.3(45)	$23/2^- \to 19/2^-$
739.3	62.5(29)	$27/2^- \to 23/2^-$
756.6	25.3(27)	$25/2^- \to 21/2^-$
793.2	20.5(16)	$39/2^- \to 35/2^-$
859.6	19.0(17)	$41/2^- \to 37/2^-$
926.1	10.7(16)	$43/2^- \to 39/2^-$
994.3	9.7(16)	$45/2^- \to 41/2^-$
1048.1	8.8(14)	$47/2^- \to 43/2^-$
1118.3	5.3(15)	$49/2^- \to 45/2^-$
1153.7	<5.0	$51/2^- \to 47/2^-$
1232.2	<5.0	$53/2^- \to 49/2^-$
1244.0	<5.0	$55/2^- \to 51/2^-$
1318.9	<5.0	$59/2^- \to 55/2^-$
1333.4	<5.0	$57/2^- \to 53/2^-$
1378.0	<5.0	$63/2^- \to 59/2^-$
1425.0	<5.0	$61/2^- \to 57/2^-$

[a]The γ-ray energies are estimated to be accurate to ± 0.3 keV for the strong transitions ($I_\gamma > 10$), rising to ± 0.6 keV for the weaker transitions.
[b]Transition linking Band 1 to Band 2.
[c]Transition depopulates the isomeric ($T_{1/2} \approx 62$ ns [32]) band-head of Band 1.

TABLE V. Energies, intensities, and proposed spin-parity assignments for the transitions assigned to Bands 2, 2a, and 3 in ^{129}Ce.

E_γ (keV)[a]	I_γ[b]	Assignment
	Bands 2, 2a dipoles	
144.6	>120	$7/2^+ \to 5/2^+$
203.6	91.0(27)	$9/2^+ \to 7/2^+$
241.8	53.5(24)	$11/2^+ \to 9/2^+$
245.0	19.3(15)	$25/2^+ \to 23/2^+$
278.4	21.5(15)	$27/2^+ \to 25/2^+$
278.7	41.1(15)	$13/2^+ \to 11/2^+$
301.8	9.1(8)	$29/2^+ \to 27/2^+$
309.5	25.1(14)	$15/2^+ \to 13/2^+$
337.1	26.0(16)	$17/2^+ \to 15/2^+$
355.5	16.9(13)	$19/2^+ \to 17/2^+$
356.6	7.1(12)	$31/2^+ \to 29/2^+$
363.1	17.6(15)	$21/2^+ \to 19/2^+$
375.4	5.3(13)	$33/2^+ \to 31/2^+$
389.0	<5.0	$23/2^+ \to 21/2^+$
	Bands 2, 2a quadrupoles	
348.7	28.4(22)	$9/2^+ \to 5/2^+$
445.9	30.9(19)	$11/2^+ \to 7/2^+$
520.6	36.0(21)	$13/2^+ \to 9/2^+$
523.5	9.6(17)	$27/2^+ \to 23/2^+$
579.9	8.6(17)	$29/2^+ \to 25/2^+$
587.5	51.5(27)	$15/2^+ \to 11/2^+$
633.9	<5.0	$25/2^+ \to 21/2^+$
646.1	49.1(29)	$17/2^+ \to 13/2^+$
658.2	7.7(15)	$31/2^+ \to 27/2^+$
692.7	38.0(26)	$19/2^+ \to 15/2^+$
718.4	39.0(23)	$21/2^+ \to 17/2^+$
731.8	8.6(22)	$33/2^+ \to 29/2^+$
752.1	7.1(19)	$23/2^+ \to 19/2^+$
793.2	<5.0	$35/2^+ \to 31/2^+$
869.8	<5.0	$37/2^+ \to 33/2^+$
871.1	<5.0	$39/2^+ \to 35/2^+$
961.0	<5.0	$41/2^+ \to 37/2^+$
961.0	<5.0	$45/2^+ \to 41/2^+$
	Band 3 dipoles	
235.2	38.0(16)	$27/2^+ \to 25/2^+$
239.8	36.5(16)	$25/2^+ \to 23/2^+$
280.7	33.6(16)	$29/2^+ \to 27/2^+$
294.2	29.9(14)	$31/2^+ \to 29/2^+$
303.2[c]	24.7(14)	$23/2^+ \to 21/2^+$
348.2	13.8(13)	$33/2^+ \to 31/2^+$
360.7	16.8(14)	$35/2^+ \to 33/2^+$
417.0	11.7((12)	$37/2^+ \to 35/2^+$
423.9	10.2(11)	$39/2^+ \to 37/2^+$
483.6	9.1(12)	$41/2^+ \to 39/2^+$
486.0	5.0(12)	$43/2^+ \to 41/2^+$
	Band 3 quadrupoles	
474.9	32.4(19)	$27/2^+ \to 23/2^+$
516.0	9.6(12)	$29/2^+ \to 25/2^+$
542.9[c]	15.3(15)	$25/2^+ \to 21/2^+$
574.9	26.5(19)	$31/2^+ \to 27/2^+$
642.6	22.3(19)	$33/2^+ \to 29/2^+$
666.1[c]	36.7(19)	$23/2^+ \to 19/2^+$
708.9	16.8(16)	$35/2^+ \to 31/2^+$

TABLE V. (*Continued.*)

E_γ (keV)[a]	I_γ[b]	Assignment
777.4	16.1(16)	$37/2^+ \to 33/2^+$
840.8	13.3(18)	$39/2^+ \to 35/2^+$
907.4	14.3(15)	$41/2^+ \to 37/2^+$
969.6	6.4(14)	$43/2^+ \to 39/2^+$
1029.8	7.1(14)	$45/2^+ \to 41/2^+$
1087.8	5.6(13)	$47/2^+ \to 43/2^+$
1140.8	<5.0	$49/2^+ \to 45/2^+$
1191.8	<5.0	$51/2^+ \to 47/2^+$
1243.7	<5.0	$53/2^+ \to 49/2^+$
1287.0	<5.0	$55/2^+ \to 51/2^+$

[a]The γ-ray energies are estimated to be accurate to ±0.3 keV for the strong transitions ($I_\gamma > 10$), rising to ±0.6 keV for the weaker transitions.
[b]The intensities are given relative to the 616.5-keV $19/2^- \to 15/2^-$ transition of Band 1 ($\equiv$100).
[c]Transition linking Band 3 to Band 2.

analogous to ^{127}Ce Band 3, could not be extended from the present data and is therefore not included in Fig. 3.

III. DISCUSSION

Woods-Saxon cranking calculations have been performed to deduce configurations for the bands in ^{127,129}Ce. In addition, $B(M1)/B(E2)$ ratios of reduced transition probabilities have been extracted and compared to a geometrical model to strengthen the configuration assignments. Finally, the results for ^{127,129}Ce are compared to other light odd-N cerium isotopes, namely ^{123}Ce [36], ^{125}Ce [37–40], ^{131}Ce [41,42], and ^{133}Ce [43].

TABLE VI. Energies, relative intensities, and proposed spin-parity assignments for the transitions assigned to Band 4 in ^{129}Ce.

E_γ (keV)[a]	I_γ[b]	Assignment
419.9	<2.0	$(13/2^- \to 9/2^-)$
547.3	5.3(5)	$(17/2^- \to 13/2^-)$
600.9	9.9(9)	$(21/2^- \to 17/2^-)$
633.9	9.3(9)	$(25/2^- \to 21/2^-)$
699.2	8.2(8)	$(29/2^- \to 25/2^-)$
774.2	7.5(8)	$(33/2^- \to 29/2^-)$
851.0	6.2(7)	$(37/2^- \to 33/2^-)$
923.4	4.8(7)	$(41/2^- \to 37/2^-)$
998.6	4.4(7)	$(45/2^- \to 41/2^-)$
1072.4	3.3(6)	$(49/2^- \to 45/2^-)$
1147.0	2.1(6)	$(53/2^- \to 49/2^-)$
1222.5	1.6(5)	$(57/2^- \to 53/2^-)$
1299.1	<1.0	$(61/2^- \to 57/2^-)$
1375.6	<1.0	$(65/2^- \to 61/2^-)$
1456.4	<1.0	$(69/2^- \to 65/2^-)$
1533.0	<1.0	$(73/2^- \to 69/2^-)$
1623.5	<1.0	$(77/2^- \to 73/2^-)$
1727.0	<1.0	$(81/2^- \to 77/2^-)$

[a]The γ-ray energies are estimated to be accurate to ±0.3 keV for the strong transitions ($I_\gamma > 4$), rising to ±1.0 keV for the weaker transitions.
[b]The intensities are given relative to the 616.5-keV $19/2^- \to 15/2^-$ transition of Band 1 ($\equiv$100).

A. Configurations assignments

Neutron levels, calculated with a Woods-Saxon single-particle potential and using the "universal parameters" [44,45], are shown in Fig. 5 as a function of quadrupole deformation, β_2. The levels are labeled with their asymptotic Nilsson quantum numbers; for clarity, the parity of the levels is not explicitly shown in Fig. 5 but is included in the following discussion, where the levels are labeled by the standard notation $[Nn_3\Lambda]\Omega^\pi$. In addition to the major shell closures at spherical shape ($\beta_2 = 0$) evident in Fig. 5 for $N = 50$ and 82, a deformed shell gap at $\beta_2 \sim 0.3$ is labeled for $N = 70$; the neutron orbitals close to this this gap provide the basis for configuration assignments to the rotational bands in ^{127}Ce ($N = 69$) and ^{129}Ce ($N = 71$). Configurations in the lighter ^{123,125}Ce isotones are also proposed.

1. *Configurations in* ^{129}Ce

The triangular $N = 70$ shell gap at $\beta_2 \sim 0.3$, labeled in Fig. 5, is bounded by three orbitals; the upsloping (with respect to β_2) $[402]5/2^+$ orbital originating from the $\nu d_{5/2}$ subshell, the downsloping $[541]1/2^-$ orbital originating from the $\nu h_{9/2}$ subshell, and the flat $[523]7/2^-$ orbital orginating from the $\nu h_{11/2}$ subshell. Three rotational bands have been established in $N = 71$ ^{129}Ce [34] based on the odd neutron occupying these particular orbitals; two bands show strongly coupled $\Delta I = 1$ behavior, consistent with the high-Ω values of the $[523]7/2^-$ (Band 1 in Fig. 3) and $[402]5/2^+$ (Band 2) orbitals, while the third band, associated with the $[541]1/2^-$ orbital (Band 4), is decoupled ($\Delta I = 2$) in nature. Furthermore, this latter band has an enhanced quadrupole deformation of $\beta_2 \sim 0.35$ [34], similar to heavier "superdeformed" cerium isotopes, albeit at high spin. This enhanced deformation is driven by the strongly downsloping nature of the $[541]1/2^-$ orbital, the first "intruding" component from the $N_{\rm osc} = 5$ $\nu h_{9/2}$ subshell that originates from above the $N = 82$ spherical shell closure. Note that for the heavier cerium isotopes $^{130-136}$Ce, superdeformation is usually associated with $\nu i_{13/2}$ intruder orbitals from the $N_{\rm osc} = 6$ shell [46,47].

2. *Configurations in* ^{127}Ce

With two neutrons less than ^{129}Ce, the $N = 69$ neutron Fermi surface for ^{127}Ce is expected to be close to the $[411]1/2^+$ ($\nu d_{3/2}$) orbital, see Fig. 5; the three bands in ^{127}Ce are thus assigned to the odd neutron occupying this orbital (Band 3 in Fig. 1), respectively, plus the $[402]5/2^+$ ($\nu d_{5/2}$, Band 2) and $[523]7/2^-$ ($\nu h_{11/2}$, Band 1) orbitals, as seen in ^{129}Ce. With $\Omega = 1/2$, the $[411]1/2^+$ state is expected to show a large signature splitting with increasing rotation. This is consistent with the properties of Band 3 in ^{127}Ce. The $[411]1/2^+$ orbital

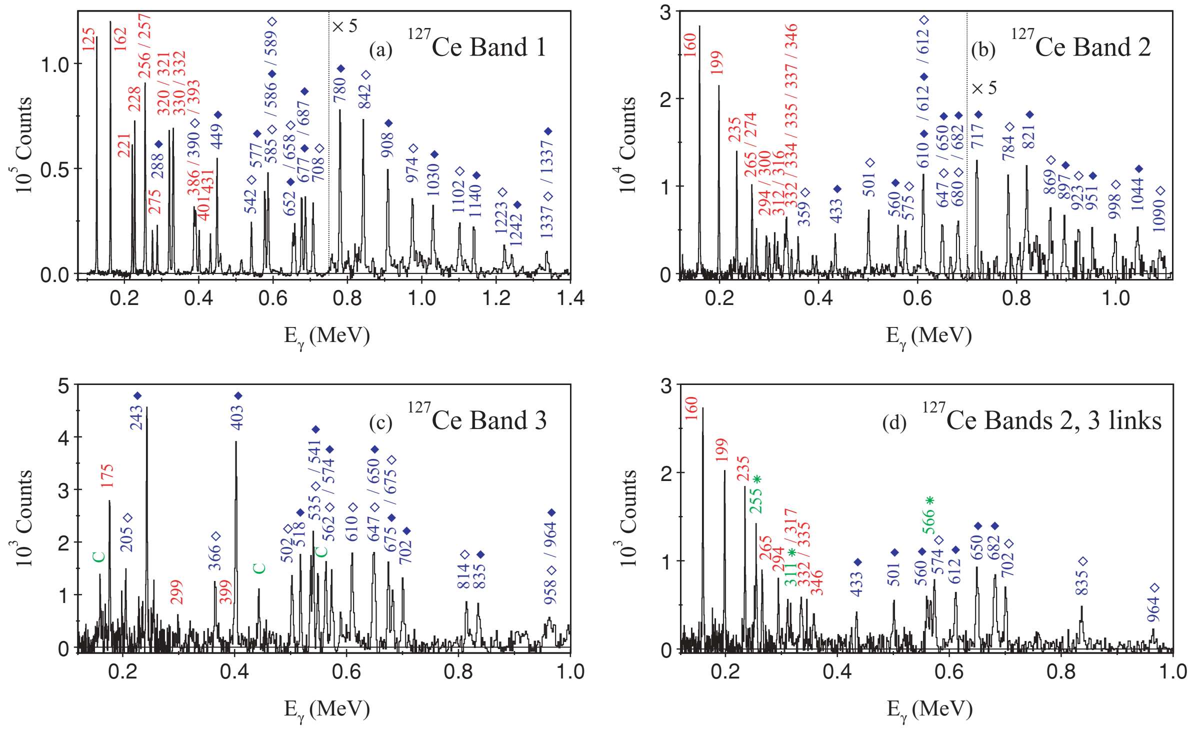

FIG. 2. (Color online) Triple-gated quadruple-coincidence spectra for the bands in ^{127}Ce, showing transitions in Band 1 (a), Band 2 (b), and Band 3 (c). In each case, a sum of "clean" gates was set on each axis of the hypercube. In each spectrum, the transitions are labeled by their energies in keV; dipole transitions are shown in red, while the two $E2$ signature components are denoted by filled and open diamonds (blue), respectively. Spectrum (d) shows the three linking transitions, denoted by an asterisk (green), between Band 2, denoted by solid diamonds (blue), and Band 3, denoted by open diamonds (blue). Contaminant peaks are labeled with "C" (green) in (c).

is at the Fermi surface in heavier superdeformed (SD) Ce isotopes at high spin; it is the "pseudospin" (hole) orbital that gives rise to "identical band" relations in the SD bands of ^{131,132}Ce [48].

3. *Configurations in* ^{125}*Ce and* ^{123}*Ce*

With a further two neutrons less, the [411]$1/2^+$ orbital is again expected to be near the $N = 67$ neutron Fermi surface for ^{125}Ce. Indeed, an analogous structure to ^{127}Ce Band 3 has been identified in ^{125}Ce [38,39], which may naturally be assigned to this configuration. Furthermore, a low-lying isomeric state with a proposed $1/2^+$ spin-parity assignment has recently been identified in ^{125}Ce [40], which would correspond to the bandhead of this orbital. With reference to Fig. 5, the two other strongly coupled bands in ^{125}Ce [38,39] are predicted to correspond to [523]$7/2^-$ ($h_{11/2}$) and [413]$5/2^+$ ($g_{7/2}$) configurations, respectively.

With a further two neutrons less, the $N = 65$ neutron Fermi surface lies close to the [532]$5/2^-$ ($h_{11/2}$) and [413]$5/2^+$ ($g_{7/2}$) orbitals; indeed, bands based on these orbitals have recently been established in ^{123}Ce [36].

B. Rotational properties of the bands in ^{127,129}Ce

Rotational properties of the bands are discussed in the following sections, including backbending, signature splitting, and $B(M1)/B(E2)$ ratios of reduced transition probabilities.

1. *Band-crossing systematics*

To discuss the nature of the rotational bands in ^{127,129}Ce in terms of quasiparticle configurations, high-spin properties of the bands are compared to cranking calculations. The experimental data are presented in Fig. 6 in terms of alignment, i_x, plots [49], as a function of rotational frequency, $\omega \approx E_\gamma/2\hbar$. A reference, based on a configuration with a frequency-dependent moment of inertia, $\mathcal{J}_{\rm ref} = \mathcal{J}_0 + \omega^2\mathcal{J}_1$, has been subtracted in each case with Harris parameters [50] $\mathcal{J}_0 = 17.0\ \hbar^2\ \text{MeV}^{-1}$ and $\mathcal{J}_1 = 25.8\ \hbar^4\ \text{MeV}^{-3}$. These values were originally obtained from a fit to the S band of ^{130}Ce over the frequency range $0.30 \leqslant \omega \leqslant 0.60$ MeV/$\hbar$ [51] and provide a suitable reference for the light cerium isotopes.

It can be seen in Fig. 6 that the bands in ^{127}Ce and ^{129}Ce all show a sharp backbend at a rotational frequency $\omega \approx 0.3$ MeV/$\hbar$, with a gain in alignment $\Delta i_x \approx 9\hbar$ in each case. Precise band-crossing frequencies, obtained from experimental Routhian plots [49], are listed in Table VII. In the case of Band 2a in ^{127}Ce, and the newly identified Band 2a in ^{129}Ce, a further gain in alignment is seen at $\omega \sim 0.45$ MeV/$\hbar$.

The results of cranked Woods-Saxon calculations, appropriate for ^{127}Ce, are shown in Fig. 7. In these calculations, the pairing strength is calculated at zero frequency and is modelled to decrease with increasing rotational frequency such that the pairing has fallen by 50% at $\omega = 0.70$ MeV/$\hbar$, as detailed in Ref. [46]. Average deformation parameters $\beta_2 = 0.280$, $\beta_4 = -0.010$, and $\gamma = 0^\circ$ were obtained from total-Routhian

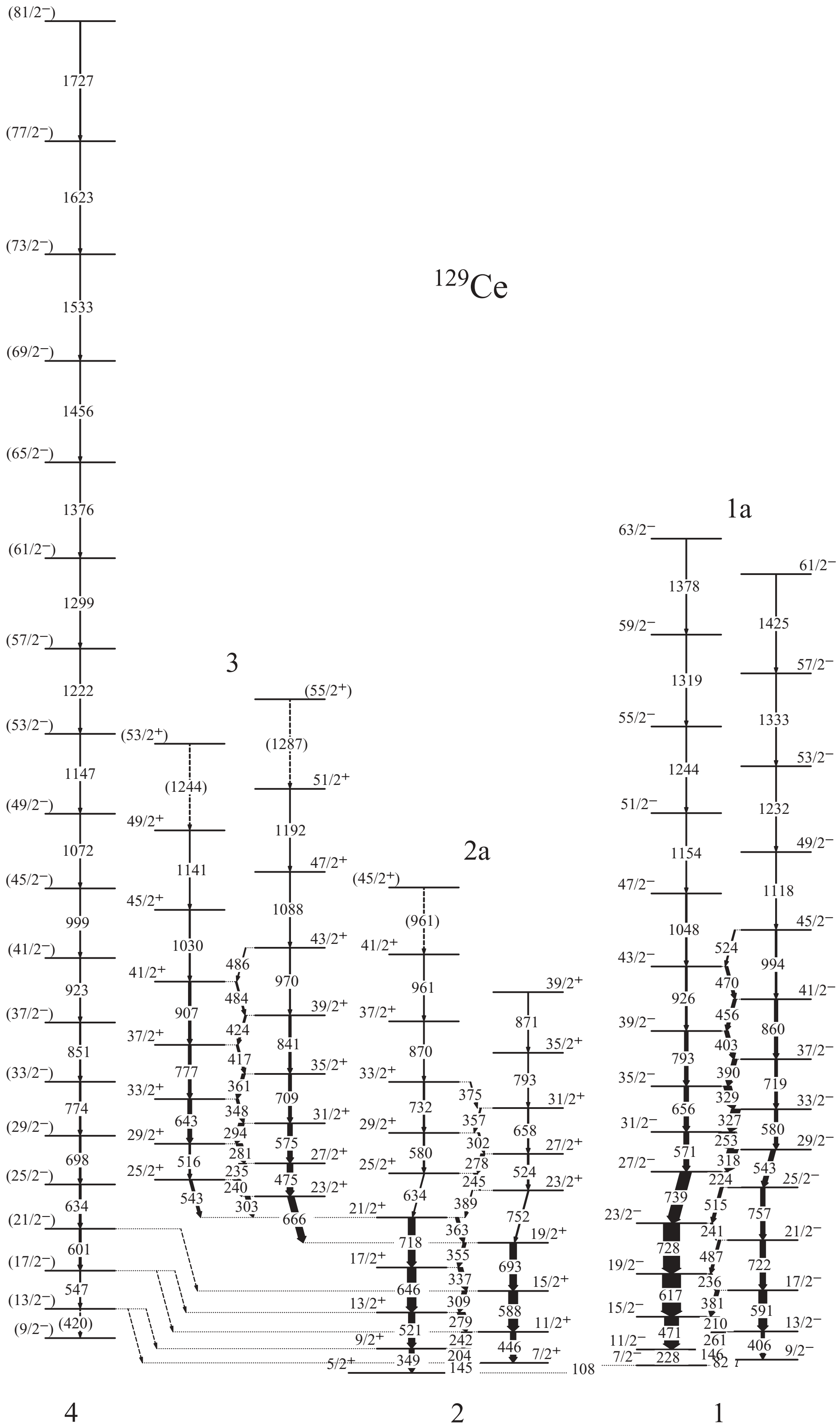

FIG. 3. Level scheme deduced for ^{129}Ce from the present work. Energies are labeled in keV and the widths of the arrows are proportional to the transition intensities.

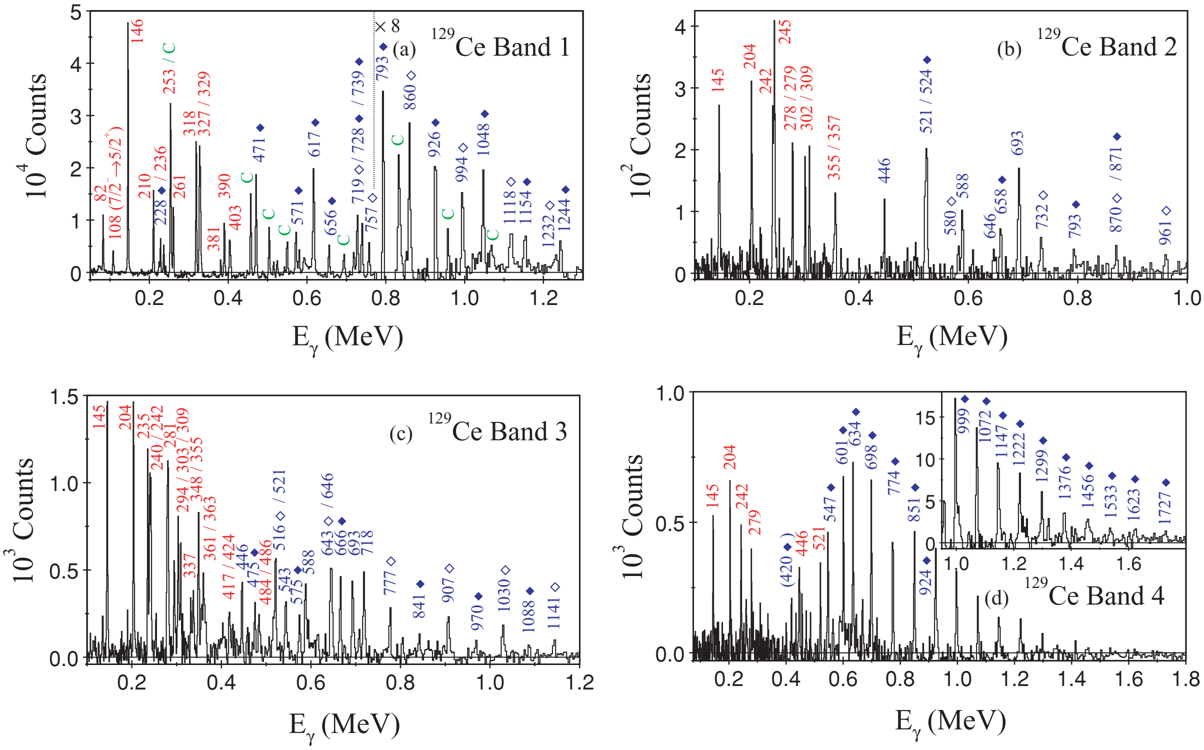

FIG. 4. (Color online) Triple-gated quadruple-coincidence spectra for the bands in ^{129}Ce, showing transitions in Band 1 (a), Band 2 (b), Band 3 (c), and Band 4 (d). In each spectrum, the transitions are labeled by their energies in keV; dipole transitions are shown in red, while the two $E2$ signature components are denoted by filled and open diamonds (blue), respectively. Contaminants from ^{130}Ce are labeled with "C" (green). The gates applied are as follows: (a) $x = y =$ Band 1 quadrupoles ($\alpha = -1/2$), $z =$ Band 1 dipoles; (b) $x = y =$ Band 2 dipoles, $z = 752$ keV; (c) $x = y =$ Band 3 dipoles, $z =$ Band 3 quadrupoles ($\alpha = +1/2$); and (d) $x = y =$ Band 4, $z = 145, 204$ keV, inset: $x = y = z =$ Band 4.

surface (TRS) calculations [46,52,53] performed for negative-parity states in this nuclide.

The labeling of the single-quasiparticle levels used in Fig. 7 is expanded in Table VIII, showing the predominant Nilsson orbitals of each state. For protons, the Fermi surface in ^{127}Ce lies almost exactly midway between the negative-parity [550]1/2$^-$ and [541]3/2$^-$ Nilsson states, such that the E, F, G, and H orbitals are almost degenerate at $\omega = 0$, see Fig. 7(a). The neutron Fermi surface lies near negative-parity [523]7/2$^-$ and positive-parity [411]1/2$^+$ and [402]5/2$^+$ Nilsson states. The results in Fig. 7(b), for an axial prolate shape, indicate that the negative-parity orbitals e and f are lowest in energy at zero frequency and should therefore provide a negative-parity ground state for ^{127}Ce. However, experimentally the corresponding $I^\pi = 7/2^-$ state lies 37 keV above the $1/2^+$

TABLE VII. First band-crossing frequencies for the bands with defined parity and signature (π,α) in ^{125,127,129}Ce.

^{125}Ce band	(π,α)	Crossing frequency (MeV/$\hbar$)
1	(−, −1/2)	0.324
1	(−, +1/2)	0.330
^{127}Ce band	(π,α)	Crossing frequency (MeV/$\hbar$)
1	(−, −1/2)	0.312
1	(−, +1/2)	0.306
2	(+, ±1/2)	0.312
^{129}Ce band	(π,α)	Crossing frequency (MeV/$\hbar$)
1	(−, −1/2)	0.325
1	(−, +1/2)	0.312
2	(+, ±1/2)	0.318
3	(+, −1/2)	0.301
3	(+, +1/2)	0.294

TABLE VIII. Quasiparticle labels appropriate for ^{127}Ce, as shown in Fig. 7. The dominant Nilsson components are given, together with the parity and signature, (π,α).

Neutrons			Protons		
Label	Nilsson state	(π,α)	Label	Nilsson state	(π,α)
a	[411]1/2$^+$	(+,+1/2)	A	[413]5/2$^+$	(+,+1/2)
b	[411]1/2$^+$	(+,−1/2)	B	[413]5/2$^+$	(+,−1/2)
c	[402]5/2$^+$	(+,+1/2)	E	[550]1/2$^-$	(−,−1/2)
d	[402]5/2$^+$	(+,−1/2)	F	[550]1/2$^-$	(−,+1/2)
e	[523]7/2$^-$	(−,−1/2)	G	[541]3/2$^-$	(−,−1/2)
f	[523]7/2$^-$	(−,+1/2)	H	[541]3/2$^-$	(−,+1/2)

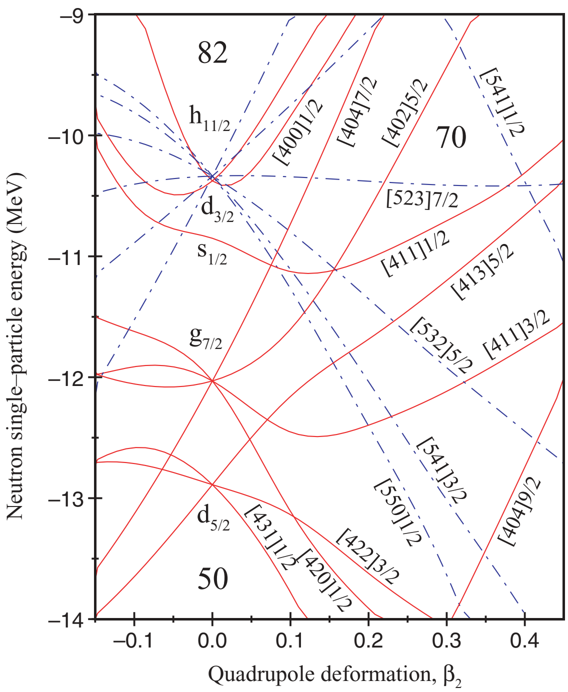

FIG. 5. (Color online) Theoretical Woods-Saxon neutron levels, shown as a function of quadrupole deformation, β_2, with $\beta_4 = \gamma = 0$. Positive-parity levels from the $N_{\rm osc} = 4$ shell are shown by solid (red) lines, while intruding negative-parity levels from the $N_{\rm osc} = 5$ shell are shown by dot-dashed (blue) lines. The levels are labeled by their asymptotic Nilsson quantum numbers, $[Nn_3\Lambda]\Omega$. Major spherical shell gaps are labeled for particle numbers 50 and 82, in addition to a deformed gap for particle number 70.

state (see Fig. 1). The relative positions of the calculated levels is highly sensitive to the triaxiality parameter γ; for instance, making γ negative increases the energy of the negative-parity states e and f relative to the positive-parity states.

The cranking calculations predict rotational-alignment frequencies of 0.30 MeV/$\hbar$ for $\pi h_{11/2}$ protons ($\omega_{\rm EF}$) and 0.40 MeV/$\hbar$ for $\nu h_{11/2}$ neutrons ($\omega_{\rm ef}$), respectively. Predicted alignment gains, $\Delta i_x = 9.0\hbar$ for protons (EF) and $\Delta i_x = 6.0\hbar$ for neutrons (ef) are obtained from the slopes of the Routhians ($i_x = -de'/d\omega$).

Cranking results for ^{129}Ce are very similar to those shown for ^{127}Ce in Fig. 7; the only difference is that the order of the a/b ([411]1/2$^+$) and c/d ([402]5/2$^+$) levels are reversed. Similar to Band 2a in ^{127}Ce, the newly identified Band 2a in ^{129}Ce shows evidence for a second backbend, at $\omega \sim 0.48$ MeV/$\hbar$, due to $h_{11/2}$ neutrons ($\omega_{\rm ef}$). However, the previously known Band 3 in ^{129}Ce does not exhibit such a feature, as is the case for Bands 1a in both ^{127,129}Ce. Blocking arguments imply that these latter bands contain a single $h_{11/2}$ neutron. Indeed, Bands 1a in ^{127,129}Ce are explicitly built on $\nu h_{11/2} \otimes \pi[h_{11/2}]^2$ configurations (eEF and fEF signature partners), while it is proposed that Band 3 in ^{129}Ce is based on a $\nu h_{11/2} \otimes \pi[h_{11/2}g_{7/2}]$ three-quasiparticle configuration (eEB and fEB signature partners). Analogous structures have been identified in the heavier ^{131}Ce [41,42] and ^{133}Ce [43] isotopes, in addition to ^{135}Nd [54]. Furthermore, the

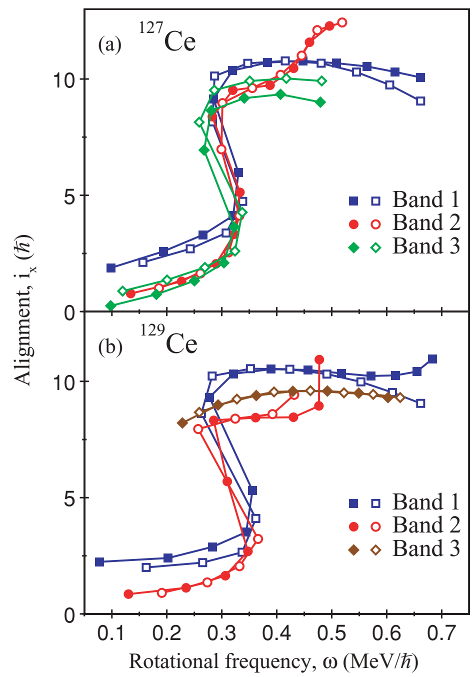

FIG. 6. (Color online) Experimental alignments, plotted as a function of rotational frequency, for bands in (a) ^{127}Ce and (b) ^{129}Ce.

$\pi[h_{11/2}g_{7/2}]$ 2-quasiparticle configuration leads to the strongly populated negative-parity sidebands in even cerium isotopes, such as ^{128}Ce [17].

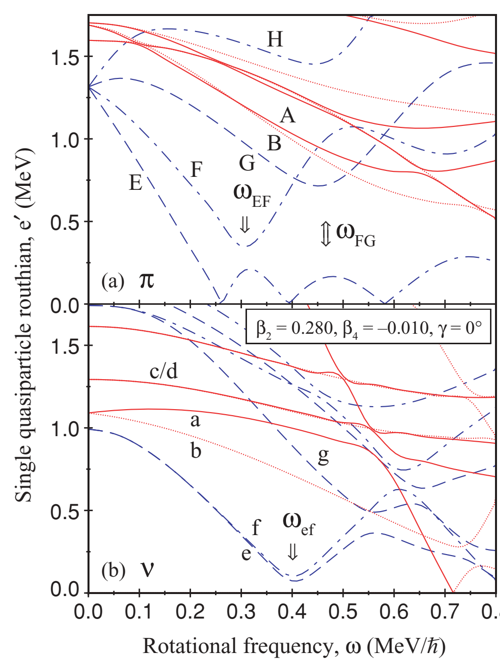

FIG. 7. (Color online) Theoretical Woods-Saxon single-quasiparticle levels for (a) protons and (b) neutrons in ^{127}Ce, shown as a function of rotational frequency. Solid lines (red) show levels with $(\pi,\alpha) = (+,+1/2)$; dotted lines (red) show $(+,-1/2)$ levels; dashed lines (blue) show $(-,-1/2)$ levels; dot-dashed lines (blue) show $(-,+1/2)$ levels. Rotational-alignment frequencies are denoted by the arrows.

2. *Signature splitting in* ^{127,129}Ce

Signature splitting, $\Delta e'$, is defined as the energy difference between the $\alpha = \pm 1/2$ components of a given single-quasiparticle configuration at a given rotational frequency, ω. Moreover, the favored signature component of a specific j-shell is given by $\alpha_f = j$ mod 2. For instance, the favored signature component of the [523]7/2$^-$ orbital ($h_{11/2}$) has $\alpha = -1/2$, and consequently spins 7/2, 11/2, 15/2, etc.. Because $\Delta e'$ is often a small quantity, it is better to extract the staggering parameter [55], as a function of spin, defined as

$$S(I) = E(I) - E(I-1) - \tfrac{1}{2}[E(I+1) - E(I) + E(I-1) - E(I-2)], \quad (1)$$

to amplify the energy differences between the signature components. Such plots of the staggering parameter are shown in Fig. 8 for bands in odd-N $^{125-129}$Ce.

For the negative-parity bands, Fig. 8(a), the staggering increases with spin up to a maximum value around spin 12$\hbar$, before decreasing to a mimimum value around spin 20$\hbar$; at higher spin, the staggering again increases. The size of the staggering at low spin is surprising because the negative-parity bands are built on high-Ω $\nu h_{11/2}$ states. Indeed, the neutron e and f orbitals appear degenerate below a frequency of 0.3 MeV/$\hbar$, as can be seen in Fig. 7(b). The staggering can be explained by invoking a degree of triaxiality, with a negative value of γ, although this is inconsistent with the present cranking calculations; Woods-Saxon TRS calculations predict nuclear shapes with $\gamma \approx 0^\circ$ for both positive- and negative-parity states in the light odd-N cerium isotopes, including ^{127,129}Ce. Although the energy minimum appears at $\gamma \approx 0^\circ$, the energy surfaces are soft with respect to γ. The TRS calculations do, however, clearly indicate nonaxial shapes for heavier odd-N cerium isotopes, approaching the $N = 82$ shell closure.

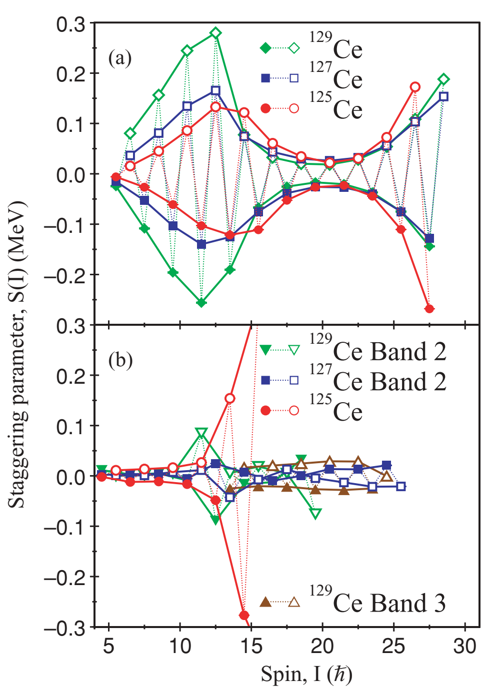

FIG. 8. (Color online) Plot of the energy staggering parameter $S(I)$ versus spin I for (a) the negative-parity and (b) the positive-parity strongly coupled bands in some odd-N cerium isotopes. The solid and open symbols represent the two signatures of each band. The spin assignments of Ref. [38] are used for the ^{125}Ce bands.

A systematic study of the staggering in negative-parity bands of odd-N Ba, Ce, Nd, and Sm ($Z = 56 - 62$) suggests a value of $\gamma \sim -20^\circ$ for ^{127}Ce and $\gamma \sim -30^\circ$ for ^{129}Ce [28]. It is the $h_{11/2}$ neutron from the upper midshell that drives the nuclear shape away from prolate. However, the rotational alignment of the EF protons from the bottom of the $h_{11/2}$ subshell will drive the nuclear shape back to prolate ($\gamma = 0^\circ$) with a consequent decrease in the staggering parameter, as seen beyond spin 12$\hbar$ in Fig. 8(a). At the highest spins, the staggering again increases suggesting a return to triaxial shapes with $\gamma < 0^\circ$.

For the strongly coupled positive-parity bands, Fig. 8(b), the staggering is much smaller at low spin because the bands are built on high-Ω orbitals ($\nu d_{5/2}$ and $\nu g_{7/2}$). However, above spin 10$\hbar$ the staggering increases, especially for ^{125}Ce. Similar to the negative-parity bands shown in Fig. 8(a), the change in the staggering may be associated with the rotational alignment of the EF protons.

3. *Electromagnetic transition strengths*

The determination of absolute $B(M1)$ and $B(E2)$ reduced transition probabilities requires the complex measurement of nuclear-level lifetimes. However, $B(M1)/B(E2)$ ratios of reduced transition probabilities may be readily extracted from experimental γ-ray branching ratios λ of competing $\Delta I = 2$ and $\Delta I = 1$ transitions depopulating a level, i.e.,

$$\frac{B(M1; I \to I-1)}{B(E2; I \to I-2)} = 0.697 \frac{[E_\gamma(I \to I-2)]^5}{[E_\gamma(I \to I-1)]^3} \times \frac{1}{\lambda} \frac{1}{[1+\delta^2]} \left[\frac{\mu_N^2}{e^2 b^2}\right], \quad (2)$$

with $\lambda = T_\gamma(I \to I-2)/T_\gamma(I \to I-1)$ and E_γ measured in MeV. Such experimental ratios of reduced transition probabilities have been extracted for the bands in ^{127,129}Ce and are shown in Fig. 9. In the present analysis, double- or triple-gated γ-ray spectra were produced using gates above the level of interest. The intensity branching ratio, λ, of the competing quadrupole and dipole transitions depopulating that level was then measured. The $E2/M1$ multipole mixing ratios were assumed to be zero; typically $\delta^2 \ll 1$ and the $B(M1)/B(E2)$ ratios are insensitive to the exact value of δ, especially in comparison to the size of the errors on the intensities.

Calculated $B(M1)/B(E2)$ ratios, using the semiclassical model of Dönau and Frauendorf [56,57], are also included in Fig. 9. The calculations have been performed with g factors taken from the Woods-Saxon cranking calculations and with average experimental alignments, listed in Table IX. The g factor of the core was taken as equal to Z/A and its quadrupole moment, Q_0, was calculated from the predicted TRS deformation parameters.

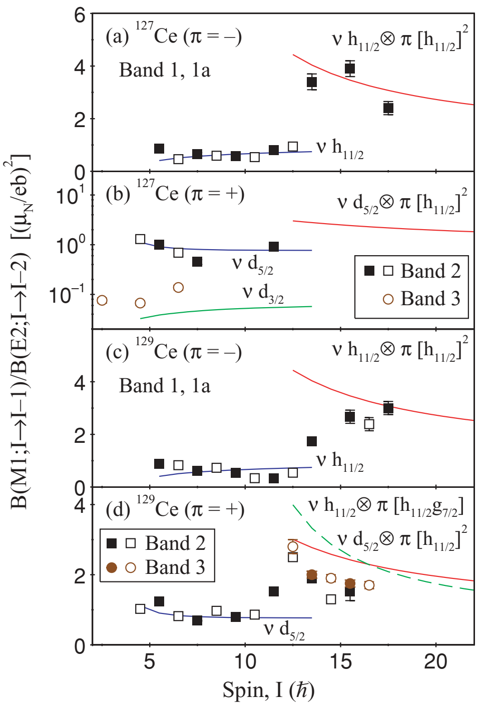

FIG. 9. (Color online) Experimental $B(M1)/B(E2)$ ratios of reduced transition probabilities for the bands in ^{127,129}Ce. The dotted lines show theoretical estimates obtained for the given configurations.

The experimental $B(M1)/B(E2)$ ratios for Band 1 in ^{127}Ce average around 0.6 $(\mu_N/e\,\text{b})^2$; those for Bands 2 and 3 average around 0.9 $(\mu_N/e\,\text{b})^2$ and 0.1 $(\mu_N/e\,\text{b})^2$, respectively. The ratios for Band 3 are much smaller than those of the other bands, reflecting the low K value of this band, which is based on the [411]1/2$^+$ ($d_{3/2}$) orbital. The experimental $B(M1)/B(E2)$ ratios for Band 1 in ^{129}Ce average around 0.6 $(\mu_N/e\,\text{b})^2$, while those of Band 2 average around 0.9 $(\mu_N/e\,\text{b})^2$, similar to the corresponding bands in ^{127}Ce.

For the case of the negative-parity Bands 1 in ^{127}Ce and ^{129}Ce, good agreement is found between the experimental and theoretical $B(M1)/B(E2)$ ratios, and a clear increase is observed around spin 12$\hbar$ when the $h_{11/2}$ protons align (Band 1 → Band 1a). Similarly, the $B(M1)/B(E2)$ ratios for the positive-parity Bands 2a and 3 in ^{129}Ce are larger than those of Band 2 at low spin, but smaller than the predictions of Fig. 9(d).

TABLE IX. Calculated Woods-Saxon single-particle g factors and experimental alignments used to calculate the $B(M1)/B(E2)$ ratios of reduced transition probabilities. The rotationally aligned EF protons were assumed to carry nine units of alignment. Dominant Nilsson components are labeled.

Label	Nilsson state	g factor	i_x
a,b	[411]1/2$^+$	1.88	1.5
c,d	[402]5/2$^+$	−0.49	0.5
e,f	[523]7/2$^-$	−0.32	2.5
A,B	[413]5/2$^+$	0.57	1.5
E,F	[550]1/2$^-$	1.60	
G,H	[541]3/2$^-$	1.48	

IV. CONCLUSION

The level structures of the odd-N ^{127}Ce and ^{129}Ce isotopes have been investigated and extended to higher spin. Several band structures are observed in each isotope and configuration assignments made through comparison with Woods-Saxon cranking calculations. In ^{127}Ce, links between the two positive-parity bands at high spin imply that the $I^\pi = 1/2^+$ bandhead of one band ($\nu d_{3/2}$) lies 7 keV below the $5/2^+$ bandhead of the other band ($\nu d_{5/2}$), and hence the ground-state spin and parity of ^{127}Ce is reassigned as $1/2^+$. This state also lies 37 keV below the $7/2^-$ bandhead of the $\nu h_{11/2}$ band. The experimental relative energies of single-particle states in nuclei away from the line of β stability provide invaluable input into current nuclear-structure theory.

The negative-parity bands in the light odd-N cerium isotopes exhibit unusually large values of signature splitting, consistent with nonaxial shapes for these structures. It is believed that this arises due to polarization of the γ-soft core by high-j neutrons from the upper $h_{11/2}$ midshell. These results provide further (indirect) evidence for static triaxial shapes in atomic nuclei.

ACKNOWLEDGMENTS

Funding for this work is acknowledged from the UK EPSRC and the French IN2P3. We thank all the crew and technical support connected with the Eurogam facility in Strasbourg, and the Euroball facility in Legnaro. R. Darlington (Daresbury) is thanked for manufacturing the targets. Finally, we are indebted to Dr. D. C. Radford for providing the RADWARE analysis codes and to Drs. W. Nazarewicz and R. Wyss for providing the Woods-Saxon cranking codes.

[1] A. Bohr and B. R. Mottelson, *Nuclear Structure*, Vol. II (W. A. Benjamin Inc., New York, 1975).
[2] G. Andersson, S. E. Larsson, G. Leander, P. Möller, S. G. Nilsson, I. Ragnarsson, S. Åberg, R. Bengtsson, J. Dudek, B. Nerlo-Pomorska, K. Pomorski, and Z. Szymański, Nucl. Phys. **A268**, 205 (1976).
[3] S. W. Ødegård *et al.*, Phys. Rev. Lett. **86**, 5866 (2001).
[4] D. R. Jensen *et al.*, Phys. Rev. Lett. **89**, 142503 (2002).
[5] P. Möller, J. R. Nix, W. D. Myers, and W. J. Swiatecki, At. Data Nucl. Data Tables **59**, 185 (1995).
[6] I. Ragnarsson, A. Sobiczewski, R. K. Sheline, S. E. Larsson, and B. Nerlo-Pomorska, Nucl. Phys. **A233**, 329 (1974).
[7] Y. S. Chen, S. Frauendorf, and G. A. Leander, Phys. Rev. C **28**, 2437 (1983).
[8] E. S. Paul *et al.*, J. Phys. G **17**, 605 (1991).
[9] S. Frauendorf and F. R. May, Phys. Lett. **B125**, 245 (1983).
[10] G. A. Leander, S. Frauendorf, and F. R. May, in *Proceedings of the Conference on High Angular Momentum Properties of Nuclei, Oak Ridge, 1982*, edited by N. R. Johnson (Harwood Academic, New York, 1983), p. 281.

[11] E. S. Paul, C. W. Beausang, D. B. Fossan, R. Ma, W. F. Piel Jr., N. Xu, L. Hildingsson, and G. A. Leander, Phys. Rev. Lett. **58**, 984 (1987).
[12] J. Simpson, Z. Phys. A **358**, 139 (1997).
[13] C. W. Beausang *et al.*, Nucl. Instrum. Methods A **313**, 37 (1992).
[14] G. Duchêne, F. A. Beck, P. J. Twin, G. de France, D. Curien, L. Han, C. W. Beausang, M. A. Bentley, P. J. Nolan, and J. Simpson, Nucl. Instrum. Methods A **432**, 90 (1999).
[15] J. Eberth, H. G. Thomas, P. von Brentano, R. M. Lieder, H. M. Jager, H. Kammerling, M. Berst, D. Gutknecht, and R. Henck, Nucl. Instrum. Methods A **369**, 135 (1996).
[16] R. Wadsworth *et al.*, Phys. Rev. C **62**, 034315 (2000).
[17] E. S. Paul *et al.*, Nucl. Phys. **A676**, 32 (2000).
[18] D. C. Radford, Nucl. Instrum. Methods A **361**, 297 (1995); Nucl. Instrum. Methods A **361**, 306 (1995).
[19] D. C. Radford, M. Cromaz, and C. J. Beyer, in *Proceedings of the Nuclear Structure 98 Conference, Gatlinburg, 1998*, edited by C. Baktash (AIP, Melville, NY, 1999), p. 570.
[20] K. Kitao and M. Oshima, Nucl. Data Sheets **77**, 1 (1996).
[21] A. N. James, T. P. Morrison, P. J. Nolan, D. Watson, K. L. Ying, K. A. Connell, and J. Simpson, Daresbury Laboratory Annual Report (1986), p. 103.
[22] B. M. Nyakó, J. Gizon, V. Barci, A. Gizon, S. André, D. Barnéoud, D. Curien, J. Genevey, and J. C. Merdinger, Z. Phys. A **334**, 513 (1989).
[23] A. Gizon *et al.*, Z. Phys. A **351**, 361 (1995).
[24] A. Osa, M. Asai, M. Koizumi, T. Sekine, S. Ichikawa, Y. Kojima, H. Yamamoto, and K. Kawade, Nucl. Phys. **588**, 185c (1995).
[25] J. Genevey, A. Gizon, D. Barnéoud, Gh. Căta-Danil, R. Béraud, A. Emsallem, C. Foin, C. F. Liang, P. Paris, and S. Viteritti, Z. Phys. A **356**, 7 (1996).
[26] A. C. Mueller, F. Buchinger, W. Klempt, E. W. Otten, R. Neugart, C. Ekström, and J. Heinemeier, Nucl. Phys. **A403**, 234 (1983).
[27] M. Shibata, H. Iimura, M. Asai, A. Osa, K. Kawade, S. Ichikawa, M. Oshima, T. Sekine, and N. Shinohara, Phys. Rev. C **65**, 024305 (2002).
[28] O. Zeidan *et al.*, Phys. Rev. C **65**, 024303 (2002).
[29] P. J. Nolan, F. A. Beck, and D. B. Fossan, Annu. Rev. Nucl. Part. Sci. **44**, 561 (1994).
[30] A. T. Semple, E. S. Paul, A. J. Boston, I. M. Hibbert, D. T. Joss, P. J. Nolan, N. J. O'Brien, C. M. Parry, S. L. Shepherd, R. Wadsworth, and R. Wyss, J. Phys. G **24**, 1125 (1998).
[31] B. Singh, R. Zywina, and R. B. Firestone, Nucl. Data Sheets **97**, 241 (2002).
[32] J. Gizon, A. Gizon, R. M. Diamond, and F. S. Stephens, Nucl. Phys. **A290**, 272 (1977).
[33] R. Aryaeinejad, D. J. G. Love, A. H. Nelson, P. J. Nolan, P. J. Smith, D. M. Todd, and P. J. Twin, J. Phys. G **10**, 955 (1984).
[34] A. Galindo-Uribarri, S. M. Mullins, D. Ward, M. Cromaz, J. DeGraaf, T. E. Drake, S. Flibotte, V. P. Janzen, D. C. Radford, and I. Ragnarsson, Phys. Rev. C **54**, R454 (1996).
[35] J. Gizon *et al.*, Nucl. Phys. **A605**, 301 (1996).
[36] J. F. Smith *et al.* (to be published).
[37] E. S. Paul *et al.*, Phys. Rev. C **58**, 801 (1998).
[38] C. M. Petrache *et al.*, Eur. Phys. J. A **14**, 439 (2002).
[39] J. F. Smith *et al.*, Phys. Rev. C **69**, 034339 (2004).
[40] B. Sun *et al.*, Eur. Phys. J. A **31**, 393 (2007).
[41] M. Palacz, Z. Sujkowski, J. Nyberg, J. Bacelar, J. Jongman, W. Urban, W. Hesselink, J. Nasser, A. Plompen, and R. Wyss, Z. Phys. A **338**, 467 (1991).
[42] E. S. Paul *et al.* (to be published).
[43] R. Ma, E. S. Paul, C. W. Beausang, S. Shi, N. Xu, and D. B. Fossan, Phys. Rev. C **36**, 2322 (1987).
[44] W. Nazarewicz, J. Dudek, R. Bengtsson, and I. Ragnarsson, Nucl. Phys. **A435**, 397 (1985).
[45] S. Cwiok, J. Dudek, W. Nazarewicz, W. Skalski, and T. Werner, Comput. Phys. Commun. **46**, 379 (1987).
[46] R. Wyss, J. Nyberg, A. Johnson, R. Bengtsson, and W. Nazarewicz, Phys. Lett. **B215**, 211 (1988).
[47] A. V. Afanasjev and I. Ragnarsson, Nucl. Phys. **A608**, 176 (1996).
[48] D. Santos *et al.*, Phys. Rev. Lett. **74**, 1708 (1995).
[49] R. Bengtsson and S. Frauendorf, Nucl. Phys. **A327**, 139 (1979).
[50] S. M. Harris, Phys. Rev. **138**, B509 (1965).
[51] D. M. Todd, R. Aryaeinejad, D. J. G. Love, A. H. Nelson, P. J. Nolan, P. J. Smith, and P. J. Twin, J. Phys. G **10**, 1407 (1984).
[52] W. Nazarewicz, G. A. Leander, and J. Dudek, Nucl. Phys. **A467**, 437 (1987).
[53] W. Nazarewicz, R. Wyss, and A. Johnson, Nucl. Phys. **A503**, 285 (1989).
[54] W. F. Piel Jr., C. W. Beausang, D. B. Fossan, L. Hildingsson, and E. S. Paul, Phys. Rev. C **35**, 959 (1987).
[55] A. J. Kreiner, M. A. J. Mariscotti, C. Baktash, E. der Mateosian, and P. Thieberger, Phys. Rev. C **23**, 748 (1981).
[56] F. Dönau and S. Frauendorf, in *Proceedings of the Conference on High Angular Momentum Properties of Nuclei, Oak Ridge, 1982*, edited by N. R. Johnson (Harwood Academic, New York, 1983), p. 143.
[57] F. Dönau, Nucl. Phys. **A471**, 469 (1987).